Combustion and Flame 226 (2021) 229–242

Contents lists available at ScienceDirect

Combustion and Flame

journal homepage: www.elsevier.com/locate/combustflame

Understanding the antagonistic effect of methanol as a component in surrogate fuel models: A case study of methanol/*n*-heptane mixtures

Yingtao Wu[a,b], Snehasish Panigrahy[b], Amrit B. Sahu[b,*], Chaimae Bariki[c], Joachim Beeckmann[c], Jinhu Liang[d,b], Ahmed A.E. Mohamed[b], Shijun Dong[b], Chenglong Tang[a], Heinz Pitsch[c], Zuohua Huang[a], Henry J. Curran[b,*]

[a] State Key Laboratory of Multiphase Flow in Power Engineering, Xi'an Jiaotong University, Xi'an 710049, China
[b] Combustion Chemistry Centre, School of Chemistry, Ryan Institute, MaREI, National University of Ireland Galway, Ireland
[c] RWTH Aachen University, Institute for Combustion Technology, Templergraben 64, 52056 Aachen, Germany
[d] School of Environmental and Safety Engineering, North University of China, Taiyuan, Shanxi Province 030051, China

ARTICLE INFO

Article history:
Received 6 September 2020
Revised 3 December 2020
Accepted 4 December 2020
Available online 15 December 2020

Keywords:
Rapid compression machine (RCM)
Methanol
n-Heptane
Ignition delay time
Laminar burning velocity
Chemical kinetics

ABSTRACT

Methanol is a widely used engine fuel, blend component, and additive. However, no systematic auto-ignition data or laminar flame speed measurements are available for kinetic studies of the effect of methanol as a blending or additive component. In this work, both ignition delay times and laminar flame speeds of pure methanol, *n*-heptane and their blends at various blending ratios were measured at engine-relevant conditions. Results show that increasing methanol in a blend promotes reactivity at high temperatures and inhibits it at low temperatures, with the crossover temperature occurring at approximately 970–980 K with it being almost independent of pressure. The experimental data measured in this work, together with those in the literature are used to validate NUIGMech1.1, which predicts well the experimental ignition delay times and laminar flame speeds of the pure fuels and their blends over a wide range of conditions. Furthermore, kinetic analyses were conducted to reveal the effects of methanol addition on the oxidation pathways of *n*-heptane and the dominant reactions determining the fuel reactivities. It is found that competition for ȮH radicals between methanol and *n*-heptane plays an important role in the auto-ignition of the fuel blends at low temperatures. At high temperatures, methanol produces higher concentrations of $H\dot{O}_2$ radicals which produce *two* ȮH radicals either through the production of H_2O_2 and its subsequent decomposition or through direct reaction with Ḣ atoms. This promotes the high temperature reactivity of methanol/*n*-heptane mixtures for ignition delay times and laminar flame speeds, respectively.

1. Introduction

Fossil fuels are the primary energy source for the ever-growing transportation sector, and their consumption has led to an increasing demand on energy supplies and has raised concerns about harmful CO_2 emissions. As a clean-burning renewable fuel [1], methanol has been widely used in internal combustion engines both as a neat fuel, in blends, and as an additive because of its tendency to lower soot and NO_x emissions [2]. Engine studies [3–5] have explored the effect of methanol addition on exhaust emissions and the auto-ignition characteristics of fuels. However, fundamental combustion research on methanol blended with petroleum fuels is limited and chemical mechanisms of its oxidation process are not well understood.

Since the cetane number of *n*-heptane is similar to that of diesel fuel (56) and its chemistry has been well studied, *n*-heptane is widely used as a single-component diesel surrogate [6–8]. Therefore, many studies have used methanol/*n*-heptane to represent methanol/diesel fuel blends. Research of laminar, premixed methanol/*n*-heptane flames [9–11] mainly focused on the effect of methanol addition on soot precursor formation in the high temperature oxidation of *n*-heptane. Xingcai et al. [3] investigated the effect of methanol addition on the auto-ignition and combustion rate of *n*-heptane in a homogeneous charge compression ignition (HCCI) engine. A brief chemical analysis was performed by simulating the evolution histories of radical species as a function

* Corresponding authors.
E-mail addresses: amribikram.sahu@nuigalway.ie, a.b.sahu@bham.ac.uk (A.B. Sahu), henry.curran@nuigalway.ie (H.J. Curran).

https://doi.org/10.1016/j.combustflame.2020.12.006

of crank angle degree using an *n*-heptane mechanism [12] coupled with a methanol model [13]. This showed that the inhibiting effect of methanol addition was attributed to the decrease in the maximum values of nC_7-ketohydroperoxide and ȮH concentrations. Xu et al. [14] and Ling et al. [15] generated skeletal models for the oxidation of methanol/*n*-heptane blends based on a detailed *n*-heptane mechanism [16]. However, both the reduced and detailed models were not validated against experimental methanol/*n*-heptane blend data, and only comparisons of the detailed and reduced model predictions were presented. Furthermore, some computational fluid dynamics studies [17,18] which attempted to explore the combustion of methanol/*n*-heptane under engine relevant conditions also demonstrated the need for an accurate kinetic model to simulate the chemistry process coupled with turbulence.

Extensive auto-ignition studies of pure methanol and pure *n*-heptane have been conducted in shock tubes [19–24] and rapid compression machines (RCM) [25–30]. Laminar flame speeds, S_L, of pure methanol and pure *n*-heptane were measured using different experimental methods and devices including the heat flux method [31–33], the counterflow configuration [34], and closed combustion vessels [8,35–37], with then existing chemistry models usually under-predicting fuel-lean and over-predicting fuel-rich flame speed mixtures for alcohols. In a work on larger alkanes by Kelley et al. [37], it was observed that the chemistry models tended to over-predict flame speeds at low pressure and fuel-lean conditions, while other studies, such as that from Comandini et al. [8] showed an over-prediction by existing models over the entire range of equivalence ratios. However, to the authors' knowledge, there are no experimental data for methanol/*n*-heptane blends for either ignition delay time (IDT) or S_L to verify the predictions of kinetic models.

For the present work, IDTs of pure methanol, pure *n*-heptane, and methanol/*n*-heptane blends at liquid volume blending ratios of 75/25, 67/33, 50/50 and 25/75 were measured in an RCM under engine-relevant conditions (air diluted, equivalence ratios $\varphi = 0.5$, 1.0, 2.0, pressures $p = 10$–30 bar). Laminar flame speeds of pure methanol and pure *n*-heptane were measured in a constant volume spherical chamber at equivalence ratios ranging from 0.8 to 1.3 at an initial temperature of 423 K and at pressures of 1 atm and 2.5 and 5.0 bar. Methanol/*n*-heptane mixtures at liquid volume blending ratios of 90/10, 80/20, and 50/50 were also investigated in the spherical chamber at $\varphi = 1.2$, at an unburned temperature of 423 K, and at 1 atm and 2.5 bar. The data were further used to validate NUIGMech1.1, including species in the range C_1–C_7. In the following sections, the experimental apparatuses are briefly described and the experimental results together with NUIGMech1.1 model predictions are presented and discussed. Moreover, sensitivity and reaction pathway analyses of the blends were conducted to determine the effects of methanol addition on the oxidation of *n*-heptane and the important reactions controlling the reactivities of their mixtures.

2. Experimental setup

2.1. NUIG RCM

The IDTs of pure methanol and methanol/*n*-heptane blends at low temperatures (approximately 640 980 K) were measured in a twin-piston RCM at NUI Galway. Details of this facility were presented previously [38,39]. Non-reactive measurements in which O_2 was replaced by N_2 were also recorded so that facility effects could be simulated, with all pressure/time histories converted into volume/time histories for use in our simulations [40,41]. One of the major uncertainties in the RCM data stems from the uncertainty of calculated temperatures at the end of compression (T_C), which is estimated to be less than 10 K in this study based on the independent parameter method published by Weber et al. [42]. The detailed calculations of T_C along with one example of the python scripts are provided as Supplementary material. An overall uncertainty of ± 20% for IDTs has been assigned based on a previous study [2] conducted using the same facilities. All of the mixtures were prepared in heated stainless-steel tanks, and the partial pressures of methanol and *n*-heptane were maintained below one-third their saturation vapor pressures. Methanol and *n*-heptane were obtained from Sigma-Aldrich at 99.5+% purity and O_2, N_2 and Ar were supplied by BOC Ireland (purity > 99.5%).

2.2. Shock tube

IDTs for pure methanol, *n*-heptane, and 50/50 methanol/*n*-heptane fuel blends were measured in the NUIG high-pressure shock tube (HPST) [43] at high temperatures, where IDTs are less than 3 ms. Details of this shock tube and the methodology used to measure the IDTs were presented previously [43]. IDTs of a stoichiometric *n*-heptane/air mixture at 10 bar and 1000–1350 K were measured in the high-pressure shock tube at North University of China (NUC), which shows good agreement with literature data [44]. Details of the NUC shock tube along with the measured IDTs are provided as Supplementary material.

Typical pressure traces and definitions of IDTs measured in the HPST and RCM are shown in Fig. 1 (more examples of pressure traces covering the domain of IDTs are provide as Supplementary material, Fig. S1). Noting that two-stage ignition behavior was also observed for the HPST experiments near the NTC temperature region similar to that described by Ciezki and Adomeit [45], and the first stage (1st) and total IDT are defined, respectively, as the time interval between 0 ms (the end of compression for RCM and the arrive of shock wave for the HPST) and the maximum rate of pressure rise due to heat release in the first stage and total ignition. The maximum pressure rise (dp/dt_{max}) behind the reflected shock prior to ignition was found to be less than 2%/ms, therefore, the system could be treated to be at constant pressure. This also confirms the limited non-ideal effects of the HPST facility on the IDT measurements. For all of the IDT measurements an uncertainty of ± 20% is assigned according to a previous study [46] using the same facilities.

2.3. RWTH combustion vessel

Laminar flame speed experiments of methanol, *n*-heptane, and methanol/*n*-heptane blends were performed in the RWTH high-pressure spherical combustion vessel [35] over a wide range of equivalence ratios (0.8 –1.3) at 1 atm and 2.5 and 5.0 bar and 423 K. A schematic of the experimental set-up is shown in Fig. 2(a). The chamber has an inner diameter of 100 mm with two quartz windows of 25 mm radius positioned on opposite sides. The outward location of the propagating flame was imaged using a dual-field-lens Schlieren arrangement with a high-speed CMOS camera (LaVision High-SpeedStar 6). The acquisition rate was set to 25 kHz with a field of view of 448 × 448 pixel^2, resulting in a magnification ratio of 11.41 px/mm. The Schlieren system consists of a pulsed-high-power LED emitting green light, an aspheric condenser lens, three spherical lenses, and two pinholes. A sequence of typical Schlieren images is provided in Fig. 2(b). All fuel/air mixtures were prepared in a separate premixing vessel using the partial pressure method. Two pressure transducers of type Keller Series 35 X HTC were used during mixture preparation with different ranges to accurately measure and control the filling process. A high voltage ignition system was used to ignite the mixture at the center of the chamber using a pair of 1 mm diameter electrodes. A third pressure transducer (Kistler) captured the pressure rise during flame propagation.

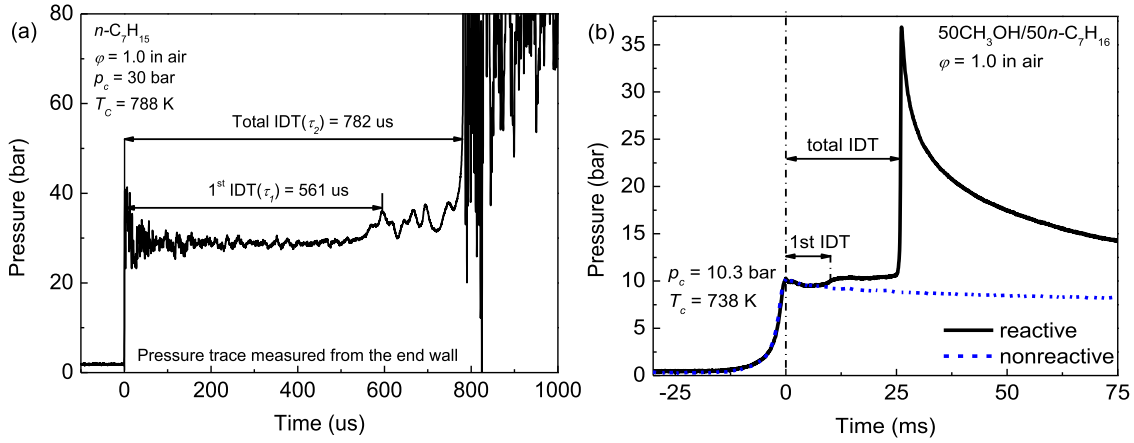

Fig. 1. Pressure traces and definitions of IDTs measured in (a) HPST and (b) RCM.

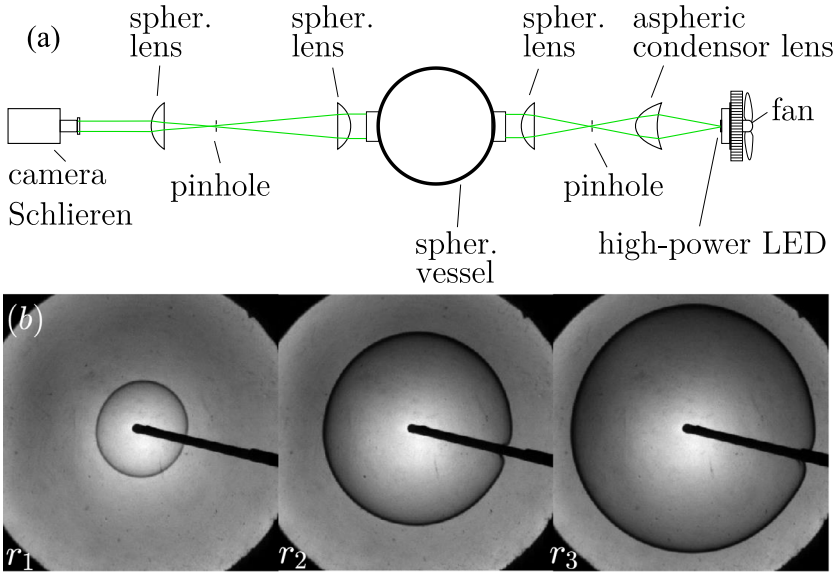

Fig. 2. (a) Schematic of RWTH experimental set-up. (b) Sequence of typical Schlieren images of methanol/air at φ = 1.0, 423 K and 1 atm. (r_1), (r_2) and (r_3) correspond to a flame radius of 0.8 cm, 1.4 cm, and 1.8 cm, respectively.

Laminar flame speed determination involves tracking the flame radius, R_f, using Schlieren images at quasi-constant pressure. The burned flame speed can be calculated as $S_b = dR_f/dt$ based on the assumption that the burned gas is stationary. The flame stretch rate is defined as $K = (2/R_f)(dR_f/dt)$. After extrapolating S_b to zero stretch using the non-linear method (S_b^0) [37], the laminar flame speed S_L is obtained through the density correction as $S_L = \sigma\ S_b^0$, where σ is the density ratio between the burned and unburned gases obtained using an equilibrium calculation.

Figure 3 represents an exemplary evolution of flame speed with respect to burnt gas as a function of flame stretch for methanol/air flames at 423 K and 1 atm at three different equivalence ratios (0.8, 1.0, and 1.3). Only images corresponding to a flame front radius greater than at least 9 mm were used to avoid ignition effects. A limit criterion for post-processing of a total pressure rise of 1% was imposed to determine the last image that should be used to derive the flame speed. Therefore, the domain of extrapolation was between 0.9 and 1.8 cm. An approach similar to that of Xiouris et al. [47] was applied to the current new dataset to estimate the uncertainty in the measured laminar flame speeds. The combined uncertainty in S_L, resulting from mixture preparation, initial temperatures, and pressures altogether with data post-processing, was

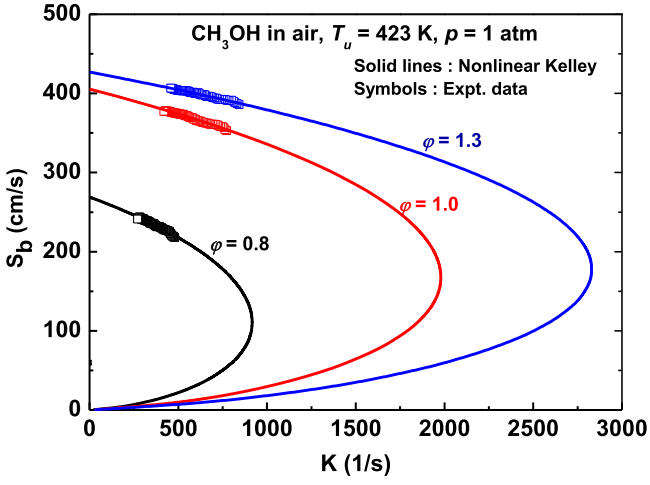

Fig. 3. Evolution of burned flame speed with respect to the burnt gas as a function of flame stretch. Nonlinear extrapolations of experimental data for methanol/air flames at 423 K and 1 atm at different equivalence ratios. The symbols at $K = 0$ represent the unstretched burned-gas flame speeds denoted as S^0_b.

Table 1
Mixture compositions studied.

Liquid volume ratio $CH_3OH/n\text{-}C_7H_{16}$	Mole ratio $CH_3OH/n\text{-}C_7H_{16}$	Equivalence ratio (φ)	% mole fraction			
			CH_3OH	$n\text{-}C_7H_{16}$	O_2	N_2/Ar
100/0	100/0	1.0	12.3	0.0	18.4	69.3
75/25	91.6/8.4	1.0	7.6	0.7	19.3	72.4
67/33	89.6/10.4	1.0	6.9	0.8	19.4	72.9
50/50	78.9/21.1	0.5	2.3	0.6	20.4	76.7
50/50	78.9/21.1	1.0	4.5	1.2	19.8	74.5
50/50	78.9/21.1	2.0	8.4	2.3	18.8	70.5
25/75	55.6/44.4	1.0	2.0	1.6	20.2	76.2
20/80	48.5/52.5	1.2	1.8	2.0	20.2	76.0
10/90	28.7/71.3	1.2	0.8	2.1	20.4	76.7
0/100	0/100	1.0	0.0	1.9	20.6	77.5

Table 2
Laminar flame speed experimental conditions.

Liquid volume ratio $CH_3OH/n\text{-}C_7H_{16}$	Equivalence ratio (φ)	Pressure	T (K)
100/0	0.8–1.3	1.0 atm, 2.5 bar	423 K
100/0	1.0	5.0 bar	423 K
0/100	0.8–1.3	1.0 atm, 2.5 bar	423 K
0/100	1.0	5.0 bar	423 K
10/90	1.2	1.0 atm, 2.5 bar	423 K
20/80	1.2	1.0 atm, 2.5 bar	423 K
50/50	1.2	1.0 atm, 2.5 bar	423 K

calculated using the residual sum of squares method. Note that at least three measurements for each condition were performed to ensure the repeatability of experiments. An uncertainty between ± 2 – 5% was obtained based on a 95% confidence interval. Radiation effects were evaluated using the correlation proposed by Yu et al. [48]. A relative error of less than 1.5% was obtained for all the conditions investigated in the present study (Fig. S2, Supplementary material). Therefore, radiative heat losses were neglected.

2.4. Mixture composition

For the IDT and S_L experiments, the blending ratios of methanol/*n*-heptane in the form of liquid volume and the corresponding mole fractions are provided in Table 1. The mole fractions of the mixture components were calculated based on the measured partial pressure of each component. If not specified, liquid volume ratios are used in the following discussion to define the blends. N_2 and/or Ar were used as the diluent gas in the RCM experiments to achieve a wide range of studied temperatures (640–980 K), while N_2 was used as the diluent gas in all of the shock tube experiments. Details of mixture compositions together with volume profiles are included in the input files provided as Supplementary material. The detailed conditions for the S_L experiments are shown in Table 2.

3. Numerical model

The detailed chemical kinetic mechanism, NUIGMech1.1, utilized here is hierarchically derived for very many major hydrocarbon and oxygenated fuels from hydrogen to C_7 combustion species encompassing an extensive work from the author's group recently [49–56]. The base chemistry employed in the detailed mechanism is based on several prior mechanisms developed at NUIG. The reaction rate constants and thermochemical properties of C_0–C_7 sub-mechanisms have been updated based on a critical evaluation of newly published experimental and theoretical studies. The kinetics for the methanol sub-mechanism used in this work is derived from Burke et al. [57]. The *n*-heptane sub-mechanism is taken from Zhang et al. [21] and has been further updated based on the rate rules published recently by Zhang et al. [58]. NUIGMech1.1 contains 2845 chemical species and 11,260 elementary reactions. Modifications made to the important reactions relevant to methanol and *n*-heptane chemistries are discussed in Section 4.3 based on kinetic analyses, and the detailed kinetic mechanism and thermodynamic files used for model predictions are provided as Supplementary material.

4. Result and discussion

4.1. Ignition delay times

IDTs for stoichiometric methanol/*n*-heptane mixtures were measured at 10, 20 and 30 bar, Fig. 4.

IDT data of pure *n*-heptane (0% CH_3OH) and methanol (100% CH_3OH) were partly taken from the literature [8,21,24,26,44,57,59] and are also presented in Fig. 4.

The IDTs measured in this study are in good agreement with those at the same conditions presented in the literature, which verifies the reliability of the current experimental data (Figs. S3 and S4 of the Supplementary material). With an increasing fraction of *n*-heptane, the reactivities of the mixtures increase significantly, especially at lower temperatures in the range 640 – 900 K. At temperatures above this, the reactivities of the different blends are very similar, and at temperatures of 970 – 980 K the reactivities of all blends become the same. The relative reactivities of methanol and *n*-heptane are then reversed at higher temperatures (> 980 K). Since differences in methanol and *n*-heptane IDTs are small at high temperatures, IDTs for only the 50/50 blends were measured in this temperature range and they fall between those of pure methanol and *n*-heptane.

At 10 bar, as shown in Fig. 4(a), at temperatures above 880 K the reactivity of the 67/33 CH_3OH/*n*-heptane mixture is very similar to that of pure CH_3OH. At lower temperatures, the 67/33 mixture shows very limited low-temperature reactivity within the available measurement range. The 50/50 and 25/75 CH_3OH/*n*-heptane mixtures show progressively more low-temperature reactivity and stronger negative temperature coefficient (NTC) behavior. At 10 bar and at T_C = 880 K, the IDT is lower by approximately a factor of four (× 4) for the 50/50 and eight (× 8) for the 25/75 CH_3OH/*n*-heptane mixtures. At the higher pressures of

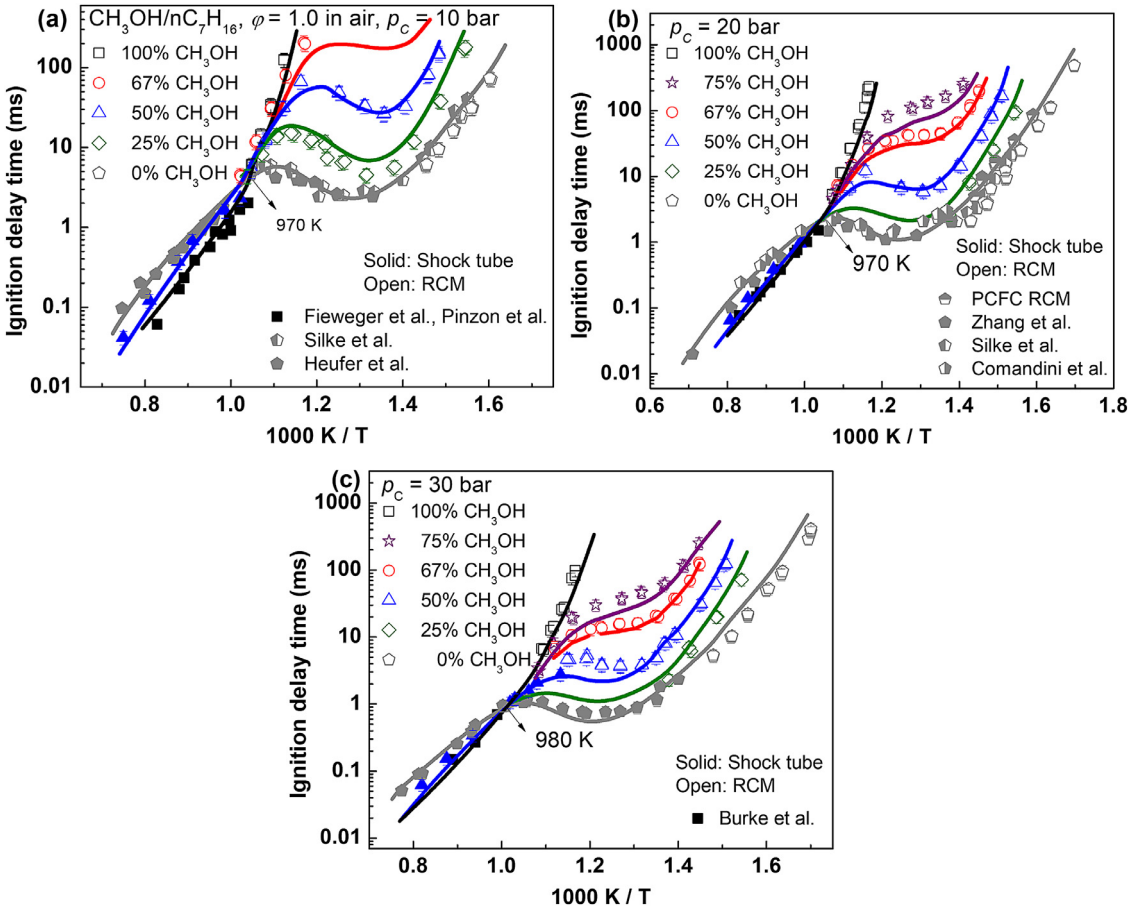

Fig. 4. IDT measurements of stoichiometric methanol/*n*-heptane blends at 10, 20, and 30 bar; solid lines are simulations using NUIGMech1.1. Some 100% CH_3OH data are from Fieweger et al. [59], Pinzón et al. [24], and Burke et al. [57]; some *n*-C_7H_{16} data are from Comandini et al. [8], Silke et al. [26], Heufer et al. [44], and Zhang et al. [21]. (For interpretation of the references to color in the legend, the reader is referred to the web version).

20 and 30 bar, the promoting effect of *n*-heptane addition on the reactivity becomes more pronounced. The presence of only 25% *n*-heptane in the mixture at 30 bar leads to a decrease in IDT of almost a factor of four at 880 K. Moreover, for the 75/25 CH_3OH/*n*-heptane mixture the reactivity is greatly enhanced, and this lowers the temperature limit at which IDTs can be measured from 850 K at 10 bar, to 710 K at 20 bar, and to 690 K at 30 bar.

As shown in Fig. 4, the IDTs of pure methanol and *n*-heptane are well captured by NUIGMech1.1 over the entire temperature range, and the auto-ignition of the 50/50 blend in the high temperature range is also well predicted. In the low temperature range, NUIGMech1.1 predicts well the promoting effect of *n*-heptane and the non-Arrhenius ignition behavior of the blends. It may be anticipated that, with an increase in *n*-heptane in a fuel blend, the mixture would show stronger NTC behavior. However, the 50/50 and 25/75 blends exhibit an equal, if not more noticeable NTC behavior compared to that observed for pure *n*-heptane, Fig. 4(a). Apart from the increasing importance of *n*-heptane chemistry in the 50/50 and 25/75 fuel blends, heat loss in the RCM experiments should also be considered. The IDTs of pure *n*-heptane in the NTC region are mainly measured in the shock tube, while the IDTs of these blend mixtures were measured using the RCM. The longer IDTs measured in the RCM tend to be more influenced by heat loss effects, and become even more pronounced near the high temperature limit of the NTC region where higher levels of Ar gas are used in the diluent. Comparisons of adiabatic, constant-volume simulations (Fig. S5) for various mixture compositions confirms that the NTC behavior becomes more pronounced with an increase of *n*-heptane in its mixtures with methanol.

It should also be noted that the transition temperature between the NTC and the high temperature domains shifts to higher temperatures with increasing amounts of *n*-C_7H_{16} in the fuel mixtures, Fig. 4. Mixtures with higher methanol concentrations exhibit an enhanced production of $H\dot{O}_2$ radicals from methanol via $\dot{C}H_2OH + O_2 \leftrightarrow CH_2O + H\dot{O}_2$ leading to higher concentrations of H_2O_2 via H-atom abstraction from stable molecules. The subsequent dissociation of H_2O_2 molecules produces two reactive $\dot{O}H$ radicals thus ending the NTC domain at relatively lower temperatures for high methanol/low *n*-heptane mixtures. This also contributes to the faster reactivity of methanol compared to *n*-heptane observed at temperatures in the range of ~960–1250 K. A detailed discussion on this is provided in Section 4.3.1 below.

IDTs of 50/50 methanol/*n*-heptane blends at different equivalence ratios and at pressures from 10 to 30 bar using the RCM are shown in Fig. 5. The reactivities of the blends are enhanced with increasing equivalence ratio, especially in the NTC region, because the reactions controlling reactivity are mostly fuel relevant ones, and thus an increase in fuel concentration leads to shorter IDTs. However, at temperatures below ~710 K (the lower limit of the NTC region), the reactivities of the $\varphi = 1.0$ and 2.0 mixtures are very similar, and differences with equivalence ratio tend to decrease at higher pressures. At 20 bar, Fig. 5(b), the IDTs of the $\varphi = 1.0$ and 2.0 mixtures are consistent and within the uncertainty of the ex-

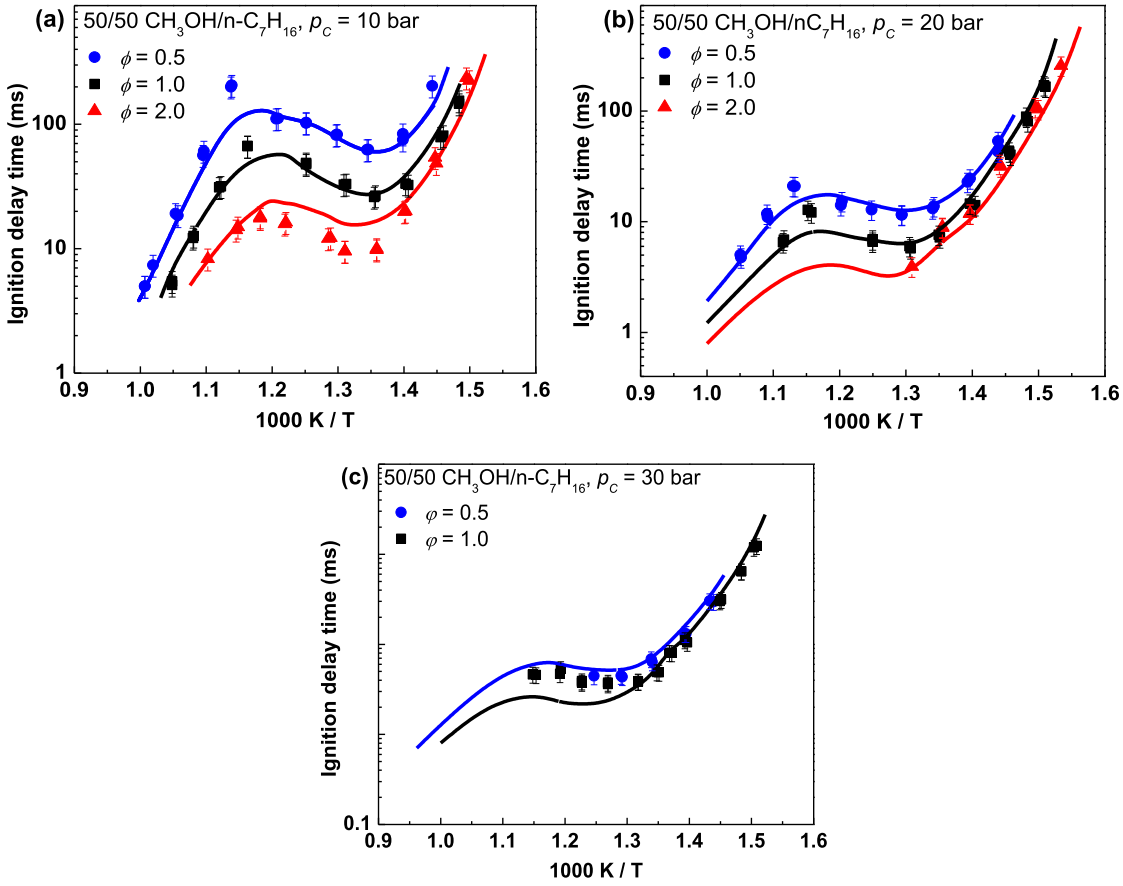

Fig. 5. IDT measurements of methanol/*n*-heptane blends at different equivalence ratios, 10–30 bar using RCM. Solid lines are simulations using NUIGMech1.1. (For interpretation of the references to color in the legend, the reader is referred to the web version).

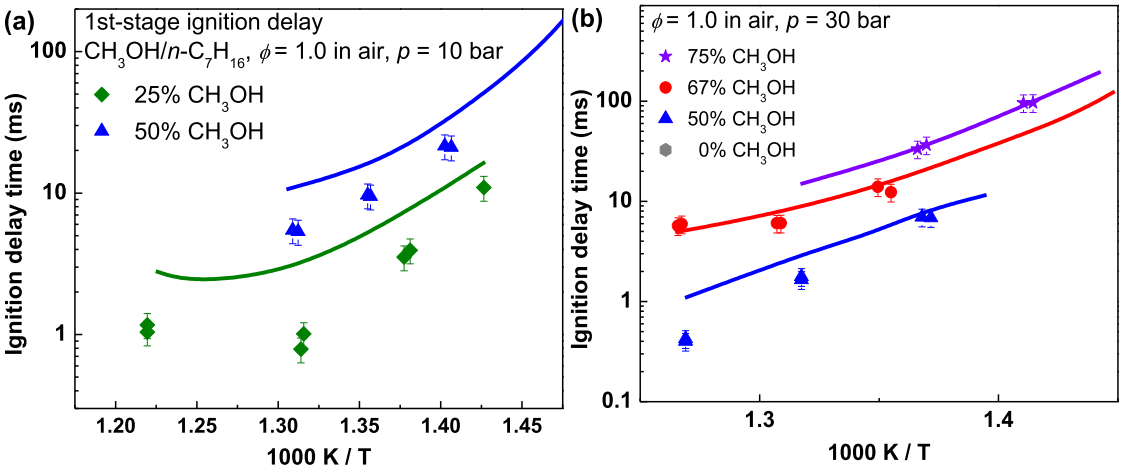

Fig. 6. 1st IDT measurements of different methanol/*n*-heptane blends at $\varphi = 1.0$, $p = 10$ and 30 bar.

periments. At 30 bar, Fig. 5(c), the IDTs of the $\varphi = 0.5$ and 1.0 mixtures are also very similar. The model shows generally good predictions for all mixtures at various pressures and equivalence ratios.

The methanol/*n*-heptane blends exhibit two-stage ignition behavior and this is also simulated using the current model, as shown in Fig. 6 (more validations are provided in Fig. S6). At 10 bar, the 1st-stage IDTs of the 25% CH_3OH blend show a mild NTC behavior similar to that for pure *n*-heptane [60], and this trend is also well captured by the model predictions, although not always quantitatively. As the fraction of *n*-heptane increases in the blends, faster 1st⁻stage ignition times are observed due to the enhanced low temperature reactivity of *n*-heptane relative to methanol. The current model generally shows good predictions of the 1st IDTs at higher pressures, while at low pressures the 1st-staged ignition times are over-predicted by a factor of 2–3. Considering the short time scales of the 1st IDTs at this condition, the kinetic model is in fair agreement with the experiments.

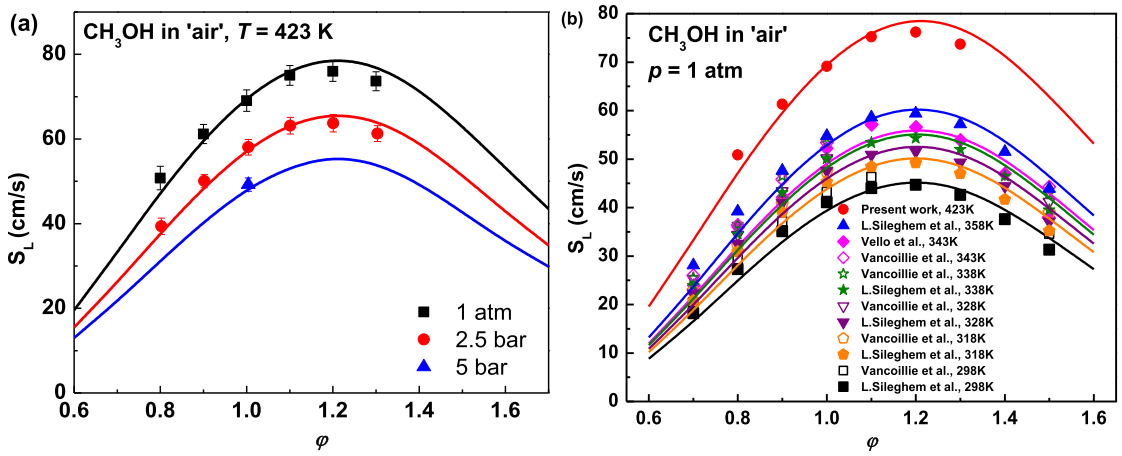

Fig. 7. Measured (symbols) and calculated (lines) laminar flame speeds of methanol/air as a function of equivalence ratio. (a) effect of pressure (p = 1 atm, 2.5 bar, 5 bar), T = 423 K; (b) effect of preheat temperature (T = 298–423 K), p = 1 atm.

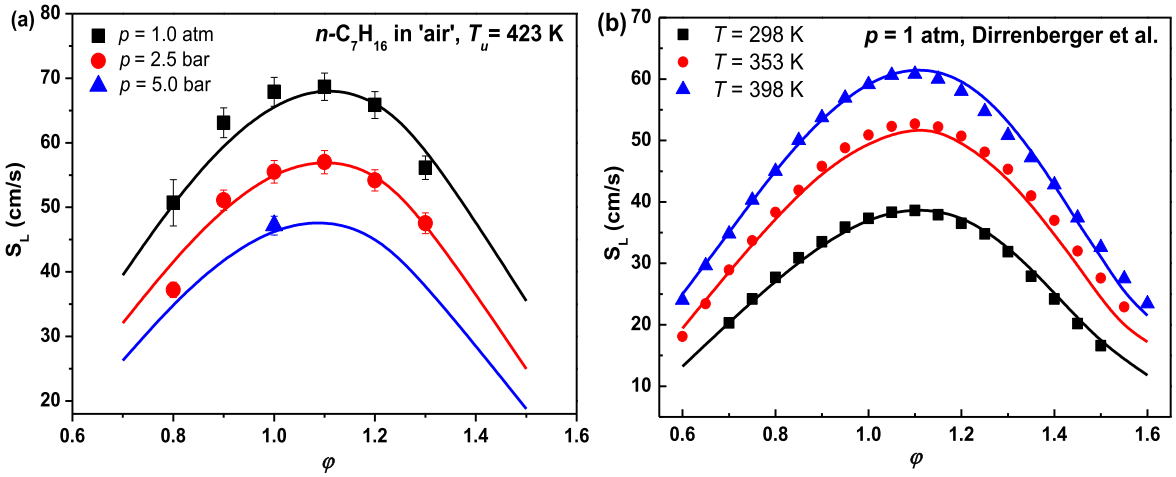

Fig. 8. Measured (symbols) and calculated (lines) laminar flame speeds of n-heptane/air at different pressures. (a) p = 1 atm, 2.5–5 bar (present work), T_u = 423 K; and at different preheat temperatures (b) T_u = 298–398 K, p = 1 atm [33].

4.2. Laminar flame speeds

Further validations of NUIGMech1.1 were performed using the laminar flame speed targets, which serves as a key parameter used to characterize combustible mixtures. New measurements were taken in the RWTH combustion vessel for methanol/air mixtures at an initial temperature of 423 K and at pressures of 1.0 atm and 2.5 and 5.0 bar, Fig. 7(a). Note that the corresponding calculations of S_L were performed using the PREMIX module of Chemkin-Pro 19.0. The current model predicts the S_Ls accurately at all equivalence ratios except at φ = 1.3 where it slightly over-predicts the experimental measurement, but it is still within the uncertainty limits. Figure 7(b) shows flame speed measurements reported in the literature [31,32,34] at various pre-heat temperatures (T_u = 298–423 K) and the predictions by the model are in good agreement with the experiments.

For n-heptane/air mixtures, Fig. 8(a) shows the current model flame speed predictions compared with measurements taken in the present study at pressures of 1 atm and 2.5 and 5.0 bar. The model simulates the measured data satisfactorily over the entire range of equivalence ratios, except at φ = 0.8 and 2.5 bar. Figure 8(b) shows the comparison of model predictions against experimental measurements reported by Dirrenberger et al. [33] performed at pre-heat temperatures varying from 298 to 398 K.

The flame speed simulations are in excellent agreement with the reported data except for the very rich mixtures (φ = 1.4–1.6) at 353 K, as shown in Fig. 8(b). Additional validations against flame speed data reported at different pressures [37] and different pre-heat conditions [61,62] are provided in the Supplementary material (Fig. S7). Overall, the laminar flame speed simulations accurately capture the experimental trends for both the fuels across a wide range of equivalence ratios, temperatures, and pressures. It is worth noting that the maximum methanol/air flame speeds occur at a slightly richer mixture (φ = 1.2) compared to n-heptane mixtures for which a maximum is typically found at φ = 1.1.

In order to investigate the effect of addition of methanol to n-heptane on laminar flame speed, measurements for methanol/n-heptane mixtures were also carried out for different blend ratios at φ = 1.2, because the differences in laminar flame speed between neat methanol and neat n-heptane are particularly large at that value. The effect of blending n-heptane to methanol is shown in Fig. 9. As expected, laminar flame speeds of the selected blends lie between those of the pure fuels. It is observed that the flame speed increases as the percentage of methanol is increased. The present model replicates this trend successfully and matches the experimental data at 1 atm and 2.5 bar very well. This effective increase in reactivity of the mixture with higher methanol concen-

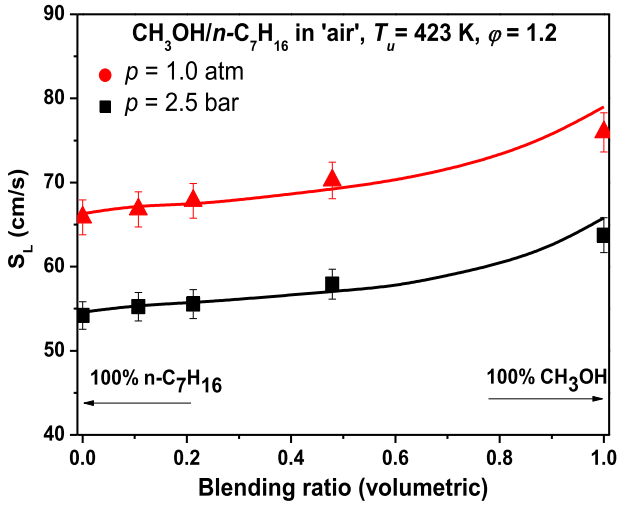

Fig. 9. Measured (symbols) laminar flame speeds of methanol/*n*-heptane blends together with the predictions of the present model (lines) at $\varphi = 1.2$, $T_u = 423$ K and $p = 1$ atm and 2.5 bar.

trations is similar to the trend observed for IDTs at the high temperature conditions presented in Fig. 3.

4.3. Kinetic analyses and discussion

4.3.1. Kinetic analyses of the autoignition of methanol/n-heptane blends

To understand the effect on the oxidation process of methanol addition to *n*-heptane, reaction flux analyses were conducted using NUIGMech1.1 for pure *n*-heptane and a 50/50 CH_3OH/*n*-C_7H_{16} mixture at $T = 800$ and 1250 K, $p = 20$ bar, at 20% *n*-heptane consumption (Fig. 10). At low temperatures, *n*-heptane oxidation is mainly initiated by H-atom abstraction reactions by $\dot{O}H$ leading to different fuel-derived radicals that later add to O_2 forming alkylperoxy radicals, ultimately leading to chain-branching. At higher temperatures, alkyl radicals tend to undergo β-scission rather than addition to O_2, Fig. 10(b). At relatively low temperatures (650–800 K), alkylperoxy radicals undergo internal H-atom transfer reactions forming hydroperoxyl-alkyl radicals.

Depending on the temperature, the concerted elimination of olefins and $H\dot{O}_2$ radicals from alkyl-peroxy radicals becomes important, reducing reactivity. In this temperature regime (650–800 K), the addition of hydroperoxyl-alkyl radicals to O_2 takes place producing hydroperoxyl-alkyl-peroxy radical. Thereafter, the rapid production of $\dot{O}H$ radicals from hydroperoxyl-alkyl-peroxy radical dissociation to carbonylhydroperoxide species, which further dissociates to produce $\dot{O}H$ and carbonyl-alkoxy radicals is the major chain branching channel at low temperatures. The other consumption pathways for hydroperoxyl-alkyl radicals at 800 K are dissociation to cyclic ethers and other β-scission products as shown in Fig. 10(a).

Compared to pure *n*-heptane, in the blend mixtures H-atom abstractions by $\dot{O}H$ radicals from *n*- heptane decrease which is mainly attributed to the competition between methanol and *n*-heptane for $\dot{O}H$ radicals. Moreover, CH_3OH oxidation produces a large fraction of the $H\dot{O}_2$ radicals through the reaction $\dot{C}H_2OH + O_2 \leftrightarrow CH_2O + H\dot{O}_2$. Therefore, adding methanol to a mixture leads to an increase in *n*-heptane consumption by $H\dot{O}_2$ radicals at intermediate temperatures (970–1250 K). The most important reaction producing $H\dot{O}_2$ radical in the methanol system is $\dot{C}H_2OH + O_2 \leftrightarrow CH_2O + H\dot{O}_2$. For this reaction, the model published by Burke et al. [57] utilized the rate constant measured by Grotheer et al. [63] in the temperature range 298 – 682 K. At high temperatures, the rate constant used by Burke et al. [57] is significantly higher than the measurements by Vandooren et al. [64] and Tsuboi and Hashimoto [65] in the temperature range 1000 – 2000 K. The current model applies a fit recommended by Baulch et al. [66] as shown in Fig. 11.

At high temperatures, fuel-derived radicals from *n*-heptane can easily decompose into small molecules via β-scission, which determines the reactivity of the fuel mixture. For methanol blended mixtures, H-atom abstractions by $\dot{C}H_3$ radicals decrease while those via $\dot{O}H$ and $H\dot{O}_2$ radicals slightly increase compared to pure *n*-heptane. This is because the increased concentration of $H\dot{O}_2$ radicals consume $\dot{C}H_3$ radicals via $\dot{C}H_3 + H\dot{O}_2 \leftrightarrow CH_3\dot{O} + \dot{O}H$. Cross-reactions, such as H-atom abstraction from *n*-C_7H_{16} by $CH_3\dot{O}$, $\dot{C}H_3$, and $\dot{C}H_2OH$ radicals contribute little to *n*-heptane consumption. The major interaction between these two fuel systems is through free radicals, among which $\dot{O}H$ and $H\dot{O}_2$ are by far the most important.

As previously discussed in Section 4.1, at temperatures below 970 K, an increase in methanol in the blends significantly increases IDTs, whereas at temperatures above this the opposite is true. To reveal the driving forces in deciding the reactivity of methanol/*n*-heptane mixtures at different temperatures, sensitivity analyses were conducted for pure *n*-heptane and the 50/50 methanol/*n*-heptane mixture at 20 bar, 800 and 1250 K. The sensitivity coefficient (S) for each reaction was calculated using:

$$S = \log(\tau_2/\tau_{0.5})/\log(2/0.5)$$

where, τ_2 and $\tau_{0.5}$ are respectively the IDTs computed with the rate constant increased or decreased by a factor of two.

A positive sensitivity coefficient indicates that this specific reaction increases the IDT, and thus decreases the system reactivity, and vice versa. According to Fig. 12(a), H-atom abstraction by $\dot{O}H$ from CH_3OH producing $\dot{C}H_2OH$ and H_2O is the most sensitive reaction inhibiting reactivity at low temperatures, while H-atom abstractions from *n*-heptane by $\dot{O}H$ are the most important in promoting mixture reactivity. At these relatively low temperatures of 800 K, *n*-heptane specific reactions such as the addition of hydroperoxyl-alkyl ($\dot{Q}OOH$) radicals to O_2 also show negative sensitivity, since they lead to the subsequent chain branching pathways. For the methanol blended mixtures, the reaction $CH_3OH + \dot{O}H \leftrightarrow \dot{C}H_2OH + H_2O$ is responsible for a significant fraction of $\dot{O}H$ radical consumption (Fig. S8) and hinders the *n*-heptane oxidation reactions initiating through H-atom abstraction by $\dot{O}H$ radicals and thus slows down the overall reactivity. The rate constant adopted for $CH_3OH + \dot{O}H \leftrightarrow \dot{C}H_2OH + H_2O$ is illustrated in Fig. S9. Furthermore, $\dot{C}H_2OH$ radicals react with O_2 producing CH_2O and $H\dot{O}_2$ radicals via $\dot{C}H_2OH + O_2 \leftrightarrow CH_2O + H\dot{O}_2$. The resultant $H\dot{O}_2$ radical undergoes a self-recombination reaction to produce H_2O_2 through $H\dot{O}_2 + H\dot{O}_2 \leftrightarrow H_2O_2 + O_2$, which inhibits reactivity at low temperatures.

As temperatures increase, H_2O_2 is also formed from H-atom abstractions from both fuels by $H\dot{O}_2$ radicals as indicated by the increase in their sensitivity coefficients in Fig. 12(b). In the case of *n*-heptane, H-atom abstraction by $H\dot{O}_2$ leads to the formation of heptyl radicals that readily decompose into smaller hydrocarbon radicals and olefins through β-scission reactions (Fig. 10(b)). However, H-atom abstraction by $H\dot{O}_2$ radicals from methanol produces $\dot{C}H_2OH$, which further generate $H\dot{O}_2$ radicals via reaction with O_2, thus sustaining the H-atom abstraction channel by $H\dot{O}_2$ as well as producing H_2O_2 and ultimately *two* $\dot{O}H$ radicals which significantly promotes the $\dot{O}H$ production rate, Fig. 12(b). Therefore, methanol blended mixtures exhibit higher reactivity at temperature above 970 K. At high temperatures competition for $H\dot{O}_2$ radicals dominates the blend's reactivity and these $H\dot{O}_2$ relevant reactions generally have large sensitivity coefficients. Unimolecular decomposition reactions of *n*-C_7H_{16} which are important in pure *n*-heptane oxidation are not sensitive in the blended mixtures.

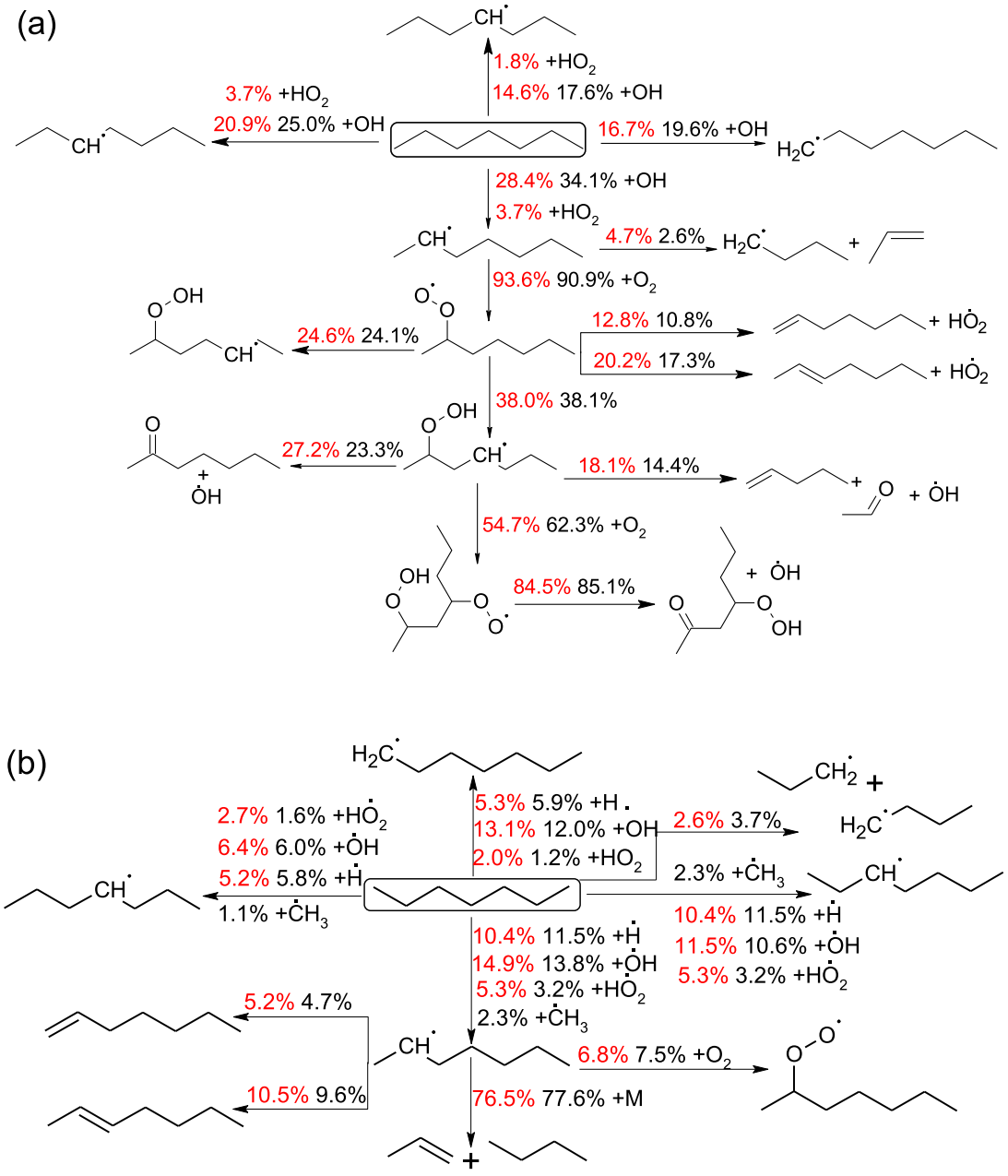

Fig. 10. Reaction flux analysis of pure *n*-heptane (black) and 50/50 CH_3OH/*n*-heptane mixture (red) at 20 bar, (a) 800 K and (b) 1250 K, where the fuel consumption rates of *n*-heptane is 20%. (For interpretation of the references to color in the legend, the reader is referred to the web version). (For interpretation of the references to color in this figure legend, the reader is referred to the web version of this article.)

4.3.2. Kinetic analyses for effect of methanol addition on n*-heptane laminar flame speeds*

The increase in flame speed observed for mixtures with higher methanol concentrations can be attributed to thermal and/or chemical effects. The former represents changes in the thermal properties such as C_p, the calorific value of the fuel or the thermal diffusivity of the mixture which lead to a rise in the peak flame temperature thereby leading to an increase in reactivity. The latter represents changes in the chemical reaction pathways leading to an increase in key radical concentrations in the reaction zone and thus, an increase in reactivity. Figure 13 shows that increasing CH_3OH composition in the fuel from 30% to 90% leads to an increase in flame speed by about 12%, while the peak flame temperature drops by ~30 K (1.3%). This comparison clarifies that the increase in flame speed caused by methanol addition is primarily due to the chemical kinetics rather than its effect on the thermal properties of the mixtures. Comparisons of the peak concentrations of key radical concentrations significantly increases (by a factor of five) as the amount of CH_3OH is varied from 30% to 90% in the blended mixtures.

Figure 14 compares the concentration profiles of CO, $\dot{O}H$, $\dot{H}$, $\dot{O}$ and $H\dot{O}_2$ for the 90/10 and 20/80 CH_3OH/*n*-C_7H_{16} mixture cases at $\varphi = 1.2$. It is observed that the peak concentrations of $\dot{O}H$ and $H\dot{O}_2$ radicals are higher for the higher methanol case. A rate of production analysis to $\dot{O}H$ radicals shows that the reaction $H\dot{O}_2 + \dot{H} \leftrightarrow \dot{O}H + \dot{O}H$ contributes to increased $\dot{O}H$ radical production, which is attributed to the rise in $H\dot{O}_2$ concentrations for the higher CH_3OH case. A comparison of the heat release rate profiles also shows that the former case exhibits a ~25% higher heat release rate compared to the latter. The comparison further confirms the domi-

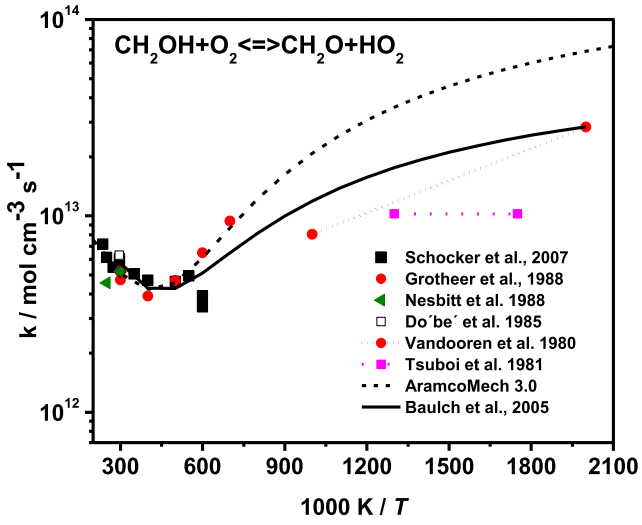

Fig. 11. Comparison of rate constant for $\dot{C}H_2OH + O_2 \leftrightarrow CH_2O + H\dot{O}_2$.

nance of chemical kinetics over thermal effects on the enhancement of flame speed.

A sensitivity analysis comparison was carried out for different *n*-heptane/methanol mixtures to identify the key reactions influencing laminar flame speeds, as shown in Fig. 15. Four mixtures containing 100% n-C_7H_{16}, 50/50 n-C_7H_{16}/CH_3OH, 20/80 n-C_7H_{16}/CH_3OH and 100% CH_3OH were considered in this study. As expected, small molecule reactions such as $\dot{H} + O_2 \leftrightarrow \ddot{O} + \dot{O}H$, $H\dot{C}O\ (+M) \leftrightarrow \dot{H} + CO\ (+M)$ and $CO + \dot{O}H \leftrightarrow CO_2 + \dot{H}$ are important reactions that enhance flame reactivity, while the reactions $\dot{H} + \dot{O}H\ (+M) \leftrightarrow H_2O\ (+M)$ and $H\dot{C}O + \dot{H} \leftrightarrow CO + H_2$ reduce flame speed predictions for all mixtures. As shown in Fig. 15, the thermal reaction between $H\dot{C}O$ and $\dot{H}$ is the most sensitive reaction inhibiting flame reactivity for all conditions. Previous NUI Galway models [21,57] implemented a temperature independent rate constant based on the experimental study by Timonen et al. [67], in which the overall rate for $H\dot{C}O + \dot{H}$ was obtained over the limited temperature of 296–418 K. However, the rate adopted in the previous models was about a factor of three lower than the measured data by Hidaka et al. [68] and Cribb et al. [69] in the temperature range of 1200–2700 K. In the present work, the rate

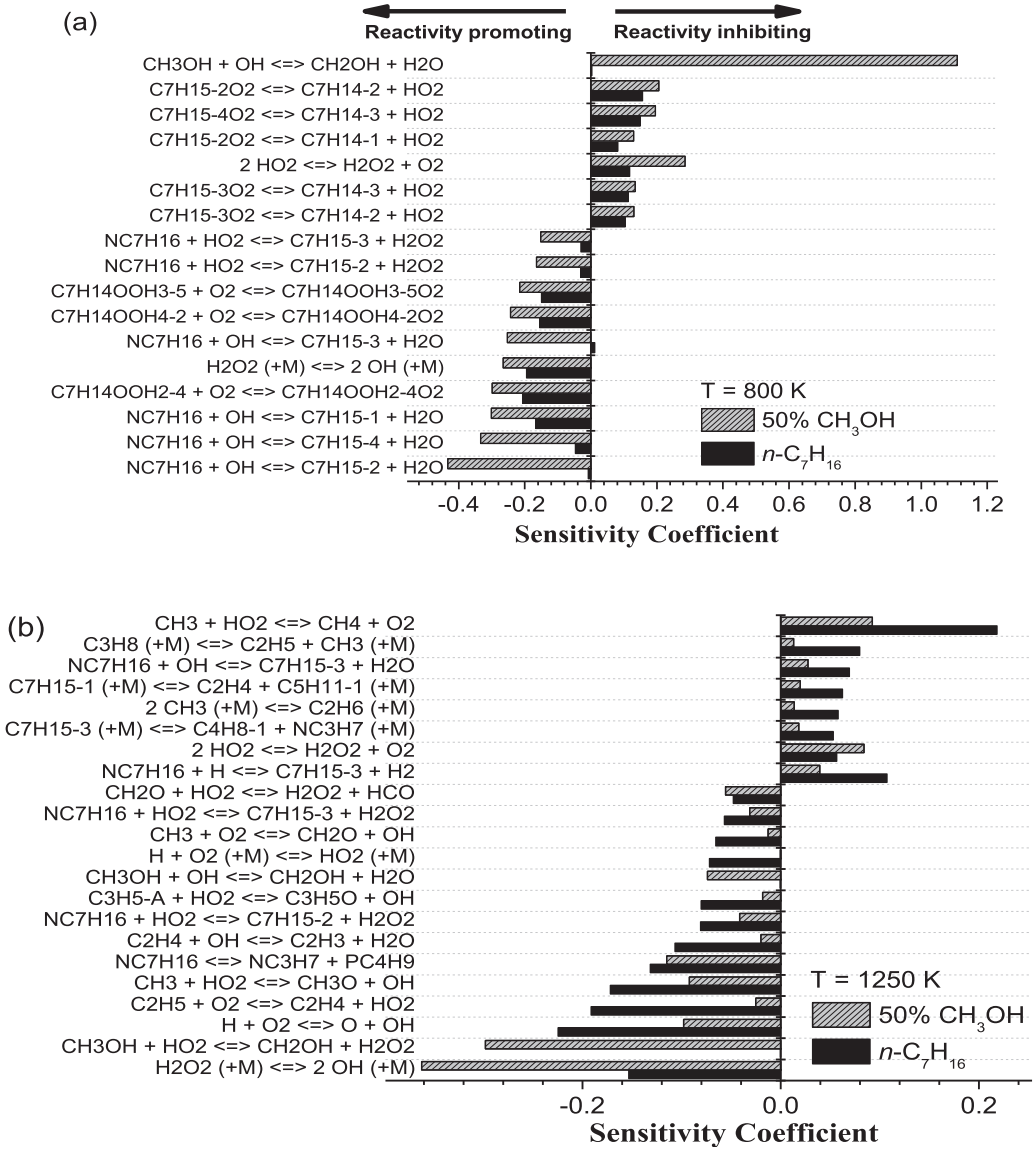

Fig. 12. Sensitivity analyses for 50/50 CH_3OH/*n*-heptane mixture at 20 bar.

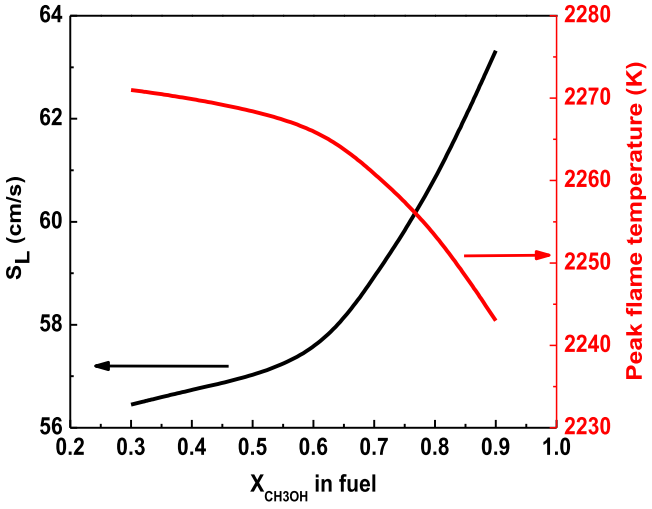

Fig. 13. Comparison of laminar flame speed and adiabatic flame temperature as a function of methanol addition to *n*-heptane/air mixtures φ= 1.2, T = 423 K and p = 1 atm.

coefficients for this reaction have been derived from the theoretical work of Harding and Wagner [70], which is in good agreement with the experimentally measured rates at higher temperatures by Hidaka et al. and Cribb et al. [68,69].

Figure 15 shows that the recombination reaction of Ḣ atoms and ȮH radicals producing water is also important for laminar flame speed predictions of all *n*-C_7H_{16}/CH_3OH mixtures. In our previous models [21,57], a pressure independent Arrhenius expression was included for this reaction based on the recommendation by Li et al. [71]. In this work, the temperature and pressure-dependent expression of rate coefficients for the Ḣ + ȮH (+M) ↔ H_2O (+M) reaction have been adopted from the high-level theoretical study of Sellevåg et al. [72], who conducted a high-level quantum chemistry study at the CASPT2/aug-cc-pVTZ level of theory.

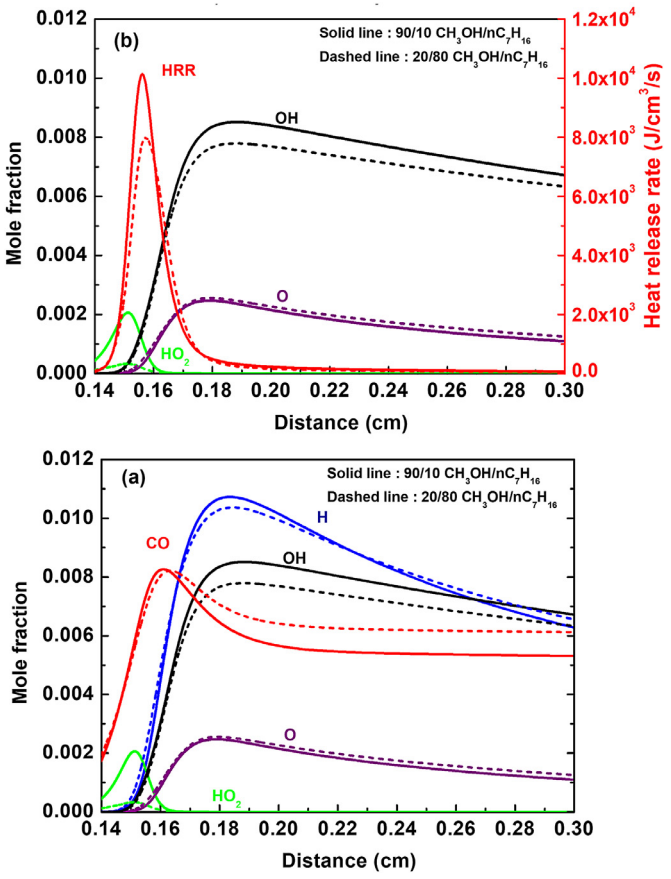

Fig. 14. Comparison of CO, ȮH, Ḣ, Ö and HȮ$_2$ concentration profiles along with heat release rate profiles between 90/10 CH_3OH/n-C_7H_{16} and 20/80 CH_3OH/n-C_7H_{16} freely propagating flames. φ = 1.2, p = 1.0 atm, T_u = 423 K.

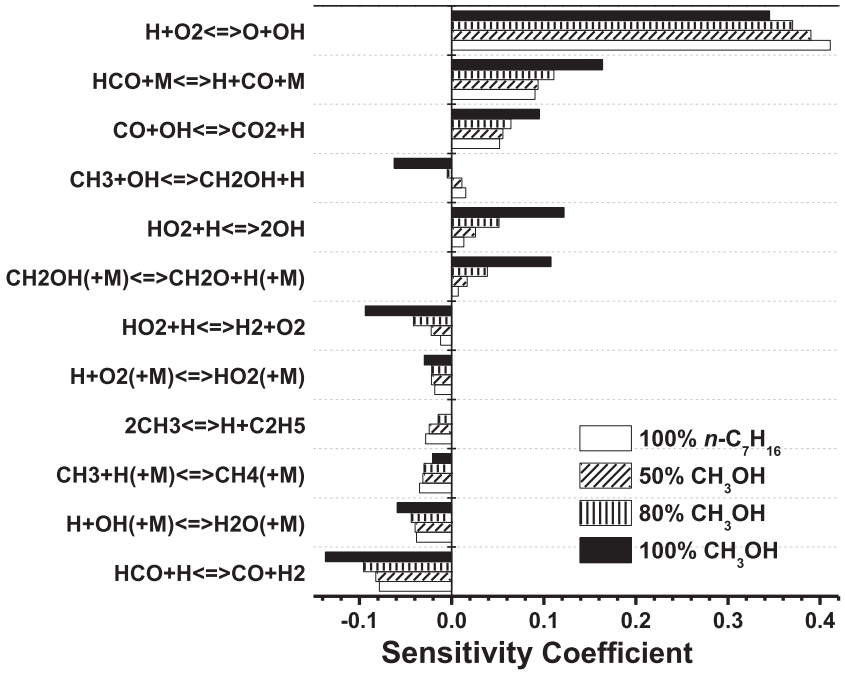

Fig. 15. Flame speed sensitivity analyses comparison for 100% *n*-C_7H_{16}, 50/50 *n*-C_7H_{16}/CH_3OH, 20/80 *n*-C_7H_{16}/CH_3OH and 100% CH_3OH mixtures at φ = 1.2, T = 423 K and p = 1 atm.

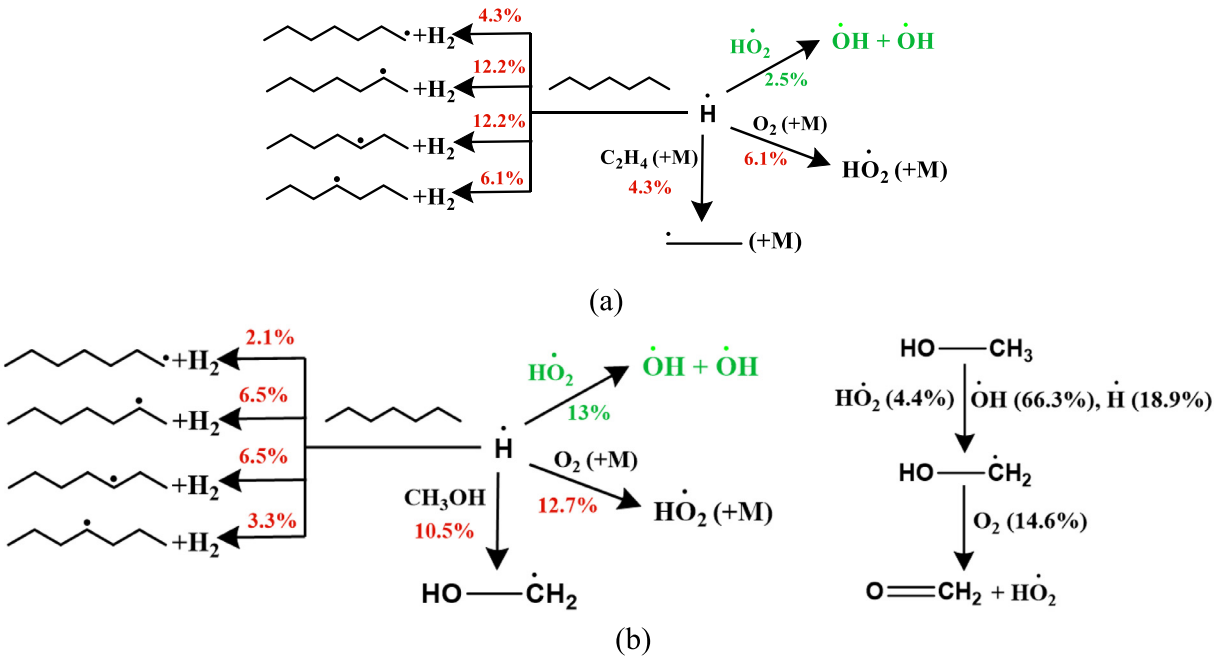

Fig. 16. Reaction flux diagram showing (a) H-atom consumption channels for 30:70, (b) H-atom consumption, HO_2 production channel from CH_3OH for 90:10 $CH_3OH/n\text{-}C_7H_{16}$ mixture.

For mixtures with high concentrations of CH_3OH (80% and 100%), unimolecular decomposition of hydroxy–methylene radical, $\dot{C}H_2OH$ (+M) ↔ CH_2O + Ḣ (+M), and its formation through the reaction $\dot{C}H_3$ + ȮH ↔ $\dot{C}H_2OH$ + Ḣ become increasingly important. The present model utilizes a rate constant that is 30% higher than the rate determined by Jasper et al. [73], which is within the uncertainty of the stated theoretical calculation. In the previous model by Burke et al. [57], the rate constant for the formation of $\dot{C}H_2OH$ and Ḣ channel was increased by a factor of two to attain better agreement with CH_3OH flame speed measurements. Additionally, $H\dot{O}_2$ + Ḣ reactions also show large sensitivity coefficients for these mixtures. The reaction producing two ȮH radicals leads to an increase in highly reactive ȮH concentrations and therefore, shows a positive sensitivity towards flame speed. Whereas the competing chain terminating channel producing H_2 and O_2 shows negative sensitivity. In order to understand the differences in the key sensitive reactions observed for these mixtures, a reaction pathway analysis was conducted.

A flux diagram comparing the consumption channels of Ḣ atoms for 30/70 and 90/10 $CH_3OH/n\text{-}C_7H_{16}$ mixture is shown in Fig. 16(a) and (b), respectively. In the case of the 30/70 mixture, ~35% of Ḣ atoms are consumed through abstraction from $n\text{-}C_7H_{16}$ producing heptyl radicals and H_2. This is followed by Ḣ atom addition to O_2 (6.1%) and C_2H_4 (4.3%) producing $H\dot{O}_2$ and $\dot{C}_2H_5$ radicals, respectively. Only 2.5% of Ḣ atoms are consumed via Ḣ + $H\dot{O}_2$ ↔ ȮH + ȮH which produces two highly reactive radicals in this mixture. Contrary to this, in the case of the 90/10 mixture, a large increase in Ḣ atom consumption through this channel is observed with approximately 13% of the Ḣ atoms reacting with $H\dot{O}_2$ radicals to produce two ȮH radicals. This increased contribution may be attributed to the rise in $H\dot{O}_2$ radical concentrations as discussed earlier.

Figure 16(b) also shows that $\dot{C}H_2OH$ which is produced by H-atom abstraction from CH_3OH, undergoes subsequent H-atom abstraction by O_2 producing CH_2O (formaldehyde) and $H\dot{O}_2$ radicals. The additional $H\dot{O}_2$ generated leads to a rise in the rate of $H\dot{O}_2$ + Ḣ ↔ ȮH + ȮH. This is in agreement with the increase in sensitivity coefficients observed in Fig. 15 for mixtures containing large concentrations of CH_3OH.

5. Conclusions

In this study, IDTs and laminar flame speeds of pure methanol, pure *n*-heptane, and their mixtures at various blending ratios were measured over a wide range of conditions covering engine relevant regimes. We provide a newly developed mechanism, NUIGMech1.1, which is validated against the experimental data measured in this work together with other available literature data, showing good agreement. The investigation also focuses on understanding the effect on the reactivity of *n*-heptane by adding methanol, which shows opposing effects at low (< 970 K) and high temperatures (> 970 K). By adding methanol, the low temperature reactivities of the blend mixtures decrease and the NTC behavior becomes less pronounced. However, at high temperatures blends with larger percentages of methanol show shorter IDTs and faster laminar flame speeds.

Kinetic analyses reveal that adding methanol to *n*-heptane leads to its competition with *n*-heptane for ȮH radicals and thus, inhibits low- and intermediate temperature *n*-heptane oxidation kinetics. Increasing the percentage of methanol in blends promotes the formation of $H\dot{O}_2$ radicals due to the reaction $\dot{C}H_2OH$ + O_2 ↔ CH_2O + $H\dot{O}_2$. At lower temperatures, while $H\dot{O}_2$ self-recombines to produce stable H_2O_2 molecule, with increasing temperature a larger percentage of $H\dot{O}_2$ radicals tend to produce H_2O_2 by H-atom abstractions from the fuel molecules, which easily decompose producing *two* reactive ȮH radicals. Since, the H-atom abstraction channel is sustained by the regeneration of $H\dot{O}_2$ via the reaction $\dot{C}H_2OH$ + O_2 ↔ CH_2O + $H\dot{O}_2$, mixture blends with methanol show shorter IDTs compared to *n*-heptane at high temperatures (> 970 K). For laminar flame speeds, the increase in $H\dot{O}_2$ concentration in the reaction zone due to methanol addition, and the subsequent reaction with Ḣ atoms producing *two* ȮH radicals also lead to an increase in flame speed measurements.

Declaration of Competing Interest

The authors declare that they have no known competing financial interests or personal relationships that could have appeared to influence the work reported in this paper.

Acknowledgments

This work is supported by the National Natural Science Foundation of China (51722603). The work at NUI Galway is supported by Science Foundation Ireland (SFI) via grant awards 15/IA/3177 and 16/SP/3829. Yingtao Wu would like to thank the financial support from the China Scholarship Council (No. 201806280105). Jinhu Liang acknowledges the support from the International Scientific Cooperation Projects of Key R&D Programs (201803D421101).

Supplementary materials

Supplementary material associated with this article can be found, in the online version, at doi:10.1016/j.combustflame.2020.12.006.

References

[1] T. Weimer, K. Schaber, M. Specht, A. Bandi, Methanol from atmospheric carbon dioxide: a liquid zero emission fuel for the future, Energy Convers. Manag. 37 (1996) 1351–1356.
[2] I.M. Atadashi, M.K. Aroua, A.A. Aziz, High quality biodiesel and its diesel engine application: a review, Renew. Sustain. Energy Rev. 14 (2010) 1999–2008.
[3] L. Xingcai, H. Yuchun, Z. Linlin, H. Zhen, Inhibition of autoignition and combustion rate for n-heptane homogeneous charge compression ignition combustion by methanol additive, Proc. Inst. Mech. Eng. Part D 220 (2006) 1629–1639.
[4] M. Canakci, C. Sayin, M. Gumus, Exhaust emissions and combustion characteristics of a direct injection (DI) diesel engine fueled with methanol–diesel fuel blends at different injection timings, Energy Fuels 22 (2008) 3709–3723.
[5] Z.H. Huang, H.B. Lu, D.M. Jiang, K. Zeng, B. Liu, J.Q. Zhang, X.B. Wang, Engine performance and emissions of a compression ignition engine operating on the diesel-methanol blends, Proc. Inst. Mech. Eng. Part D – J. Autom. Eng. 218 (2004) 435–447.
[6] J. Wullenkord, I. Graf, M. Baroncelli, D. Felsmann, L. Cai, H. Pitsch, K. Kohse-Höinghaus, Laminar premixed and non-premixed flame investigation on the influence of dimethyl ether addition on n-heptane combustion, Combust. Flame 212 (2020) 323–336.
[7] H.J. Curran, E.M. Fisher, P.A. Glaude, N.M. Marinov, W.J. Pitz, C.K. Westbrook, P.F. Flynn, R.P. Durrett, A.O. zur Loye, O.C. Akinyemi, F.L. Dryer. Sponsor Org.: US Department of Energy (US). Detailed chemical kinetic modeling of diesel combustion with oxygenated fuels. 2000-01-11 2000; United States. p.
[8] A. Comandini, N. Chaumeix, J.D. Maclean, G. Ciccarelli, Combustion properties of n-heptane/hydrogen mixtures, Int. J. Hydrogen Energy 44 (2019) 2039–2052.
[9] F. Inal, S.A. Senkan, Effects of oxygenate concentration on species mole fractions in premixed n-heptane flames, Fuel 84 (2005) 495–503.
[10] G. Chen, W. Yu, X. Jiang, Z.H. Huang, Z.D. Wang, Z.J. Cheng, Experimental and modeling study on the influences of methanol on premixed fuel-rich n-heptane flames, Fuel 103 (2013) 467–472.
[11] G. Hu, S. Liao, Z. Zuo, K. Wang, Z. Zhu, Kinetic effects of methanol addition on the formation and consumption of formaldehyde and benzene in premixed n-heptane/air flames, J. Energy Resour. Technol. 140 (2018) 072205–1-10.
[12] H.J. Curran, P. Gaffuri, W.J. Pitz, C.K. Westbrook, A comprehensive modeling study of n-heptane oxidation, Combust. Flame 114 (1998) 149–177.
[13] C.K. Westbrook, F.L. Dryer, Comprehensive mechanism for methanol oxidation, Combust. Sci. Technol. 20 (1979) 125–140.
[14] H. Xu, C. Yao, G. Xu, Chemical kinetic mechanism and a skeletal model for oxidation of n-heptane/methanol fuel blends, Fuel 93 (2012) 625–631.
[15] X.C. Ling, F. Wu, D.W. Yao, A reduced combustion kinetic model for the methanol-gasoline blended fuels on SI engines, Sci. China-Technol. Sci. 59 (2016) 81–92.
[16] M. Mehl, W.J. Pitz, C.K. Westbrook, H.J. Curran, Kinetic modeling of gasoline surrogate components and mixtures under engine conditions, Proc. Combust. Inst. 33 (2011) 193–200.
[17] S. Hu, C. Gong, X.-.S. Bai, Dual fuel combustion of n-heptane/methanol-air-EGR mixtures, Energy Procedia 105 (2017) 4943–4948.
[18] G.-.L. Xu, C.-.D. Yao, C.J. Rutland, Simulations of diesel–methanol dual-fuel engine combustion with large eddy simulation and Reynolds-averaged Navier–Stokes model, Int. J. Engine Res. 15 (2014) 751–769.
[19] J. Herzler, L. Jerig, P. Roth, Shock tube study of the ignition of lean n-heptane/air mixtures at intermediate temperatures and high pressures, Proc. Combust. Inst. 30 (2005) 1147–1153.
[20] D.F. Davidson, Z. Hong, G.L. Pilla, A. Farooq, R.D. Cook, R.K. Hanson, Multi-species time-history measurements during n-heptane oxidation behind reflected shock waves, Combust. Flame 157 (2010) 1899–1905.
[21] K. Zhang, C. Banyon, J. Bugler, H.J. Curran, A. Rodriguez, O. Herbinet, F. Battin-Leclerc, C. B'Chir, K.A. Heufer, An updated experimental and kinetic modeling study of n-heptane oxidation, Combust. Flame 172 (2016) 116–135.
[22] D. Zhang, Y. Wang, C. Zhang, P. Li, X. Li, Experimental and numerical investigation of vitiation effects on the auto-ignition of n-heptane at high temperatures, Energy 174 (2019) 922–931.
[23] K.E. Noorani, B. Akih-Kumgeh, J.M. Bergthorson, Comparative high temperature shock tube ignition of C1−C4 primary alcohols, Energy Fuels 24 (2010) 5834–5843.
[24] L.T. Pinzón, O. Mathieu, C.R. Mulvihill, I. Schoegl, E.L. Petersen, Ignition delay time and H2O measurements during methanol oxidation behind reflected shock waves, Combust. Flame 203 (2019) 143–156.
[25] R. Minetti, M. Carlier, M. Ribaucour, E. Therssen, L.R. Sochet, A rapid compression machine investigation of oxidation and auto-ignition of n-heptane: measurements and modeling, Combust. Flame 102 (1995) 298–309.
[26] E.J. Silke, H.J. Curran, J.M. Simmie, The influence of fuel structure on combustion as demonstrated by the isomers of heptane: a rapid compression machine study, Proc. Combust. Inst. 30 (2005) 2639–2647.
[27] A. Cox, J.F. Griffiths, C. Mohamed, H.J. Curran, W.J. Pitz, C.K. Westbrook, Extents of alkane combustion during rapid compression leading to single-and two-stage ignition, Symp. (Int.) Combust. 26 (1996) 2685–2692.
[28] Y. Wu, Y. Liu, C. Tang, Z. Huang, Ignition delay times measurement and kinetic modeling studies of 1-heptene, 2-heptene and n-heptane at low to intermediate temperatures by using a rapid compression machine, Combust. Flame 197 (2018) 30–40.
[29] K. Kumar, C.-.J. Sung, Autoignition of methanol: experiments and computations, Int. J. Chem. Kinet. 43 (2011) 175–184.
[30] H. Wang, R. Fang, B.W. Weber, C.-.J. Sung, An experimental and modeling study of dimethyl ether/methanol blends autoignition at low temperature, Combust. Flame 198 (2018) 89–99.
[31] L. Sileghem, V.A. Alekseev, J. Vancoillie, E.J.K. Nilsson, S. Verhelst, A.A. Konnov, Laminar burning velocities of primary reference fuels and simple alcohols, Fuel 115 (2014) 32–40.
[32] J. Vancoillie, M. Christensen, E.J.K. Nilsson, S. Verhelst, A.A. Konnov, The effects of dilution with nitrogen and steam on the laminar burning velocity of methanol at room and elevated temperatures, Fuel 105 (2013) 732–738.
[33] P. Dirrenberger, P.A. Glaude, R. Bounaceur, H. Le Gall, A.P. da Cruz, A.A. Konnov, F. Battin-Leclerc, Laminar burning velocity of gasolines with addition of ethanol, Fuel 115 (2014) 162–169.
[34] P.S. Veloo, Y.L. Wang, F.N. Egolfopoulos, C.K. Westbrook, A comparative experimental and computational study of methanol, ethanol, and n-butanol flames, Combust. Flame 157 (2010) 1989–2004.
[35] J. Beeckmann, L. Cai, H. Pitsch, Experimental investigation of the laminar burning velocities of methanol, ethanol, n-propanol, and n-butanol at high pressure, Fuel 117 (2014) 340–350.
[36] X. Zhang, G. Wang, J. Zou, Y. Li, W. Li, T. Li, H. Jin, Z. Zhou, Y.-.Y. Lee, Investigation on the oxidation chemistry of methanol in laminar premixed flames, Combust. Flame 180 (2017) 20–31.
[37] A.P. Kelley, A.J. Smallbone, D.L. Zhu, C.K. Law, Laminar flame speeds of C5 to C8 n-alkanes at elevated pressures: experimental determination, fuel similarity, and stretch sensitivity, Proc. Combust. Inst. 33 (2011) 963–970.
[38] D. Darcy, H. Nakamura, C.J. Tobin, M. Mehl, W.K. Metcalfe, W.J. Pitz, C.K. Westbrook, H.J. Curran, A high-pressure rapid compression machine study of n-propylbenzene ignition, Combust. Flame 161 (2014) 65–74.
[39] Y. Zhang, H. El-Merhubi, B. Lefort, L. Le Moyne, H.J. Curran, A. Kéromnès, Probing the low-temperature chemistry of ethanol via the addition of dimethyl ether, Combust. Flame 190 (2018) 74–86.
[40] S.M. Sarathy, S. Park, B.W. Weber, W. Wang, P.S. Veloo, A.C. Davis, C. Togbe, C.K. Westbrook, O. Park, G. Dayma, Z. Luo, M.A. Oehlschlaeger, F.N. Egolfopoulos, T. Lu, W.J. Pitz, C.-.J. Sung, P. Dagaut, A comprehensive experimental and modeling study of iso-pentanol combustion, Combust. Flame 160 (2013) 2712–2728.
[41] B.W. Weber, C.-.J. Sung, Comparative autoignition trends in butanol isomers at elevated pressure, Energy Fuels 27 (2013) 1688–1698.
[42] B.W. Weber, C.J. Sung, M.W. Renfro, On the uncertainty of temperature estimation in a rapid compression machine, Combust. Flame 162 (2015) 2518–2528.
[43] H. Nakamura, D. Darcy, M. Mehl, C.J. Tobin, W.K. Metcalfe, W.J. Pitz, C.K. Westbrook, H.J. Curran, An experimental and modeling study of shock tube and rapid compression machine ignition of n-butylbenzene/air mixtures, Combust. Flame 161 (2014) 49–64.
[44] K.A. Heufer, H. Olivier, Determination of ignition delay times of different hydrocarbons in a new high pressure shock tube, Shock Waves 20 (2010) 307–316.
[45] H.K. Ciezki, G. Adomeit, Shock-tube investigation of self-ignition of n-heptane-air mixtures under engine relevant conditions, Combust. Flame 93 (1993) 421–433.
[46] Y. Li, C.-.W. Zhou, H.J. Curran, An extensive experimental and modeling study of 1-butene oxidation, Combust. Flame 181 (2017) 198–213.
[47] C. Xiouris, T. Ye, J. Jayachandran, F.N. Egolfopoulos, Laminar flame speeds under engine-relevant conditions: uncertainty quantification and minimization in spherically expanding flame experiments, Combust. Flame 163 (2016) 270–283.
[48] H. Yu, W. Han, J. Santner, X. Gou, C.H. Sohn, Y. Ju, Z. Chen, Radiation-induced uncertainty in laminar flame speed measured from propagating spherical flames, Combust. Flame 161 (2014) 2815–2824.
[49] M. Baigmohammadi, V. Patel, S. Martinez, S. Panigrahy, A. Ramalingam, U. Burke, K.P. Somers, K.A. Heufer, A. Pekalski, H.J. Curran, A comprehensive

experimental and simulation study of ignition delay time characteristics of single fuel C1–C2 hydrocarbons over a wide range of temperatures, pressures, equivalence ratios, and dilutions, Energy Fuels 34 (2020) 3755–3771.
[50] M. Baigmohammadi, V. Patel, S. Nagaraja, A. Ramalingam, S. Martinez, S. Panigrahy, A.A.E.-S. Mohamed, K.P. Somers, U. Burke, K.A. Heufer, A. Pekalski, H.J. Curran, Comprehensive experimental and simulation study of the ignition delay time characteristics of binary blended methane, ethane, and ethylene over a wide range of temperature, pressure, equivalence ratio, and dilution, Energy Fuels 34 (2020) 8808–8823.
[51] S. Nagaraja, J. Liang, S. Dong, S. Panigrahy, A. Sahu, G. Kukkadapu, S.W. Wangon, W.J. Pitz, H.J. Curran, A hierarchical single-pulse shock tube pyrolysis study of C2–C6 1-alkenes, Combust. Flame 219 (2020) 456–466.
[52] A. Mohamed, S. Panigrahy, A. Sahu, G. Bourque, H.J. Curran, An experimental and modeling study of the auto-ignition of natural gas blends containing C1–C7 n-alkanes, Proc. Combust. Inst. 38 (2020), doi:10.1016/j.proci.2020.06.015.
[53] S. Nagaraja, J. Power, G. Kukkadapu, S. Dong, S.W. Wangon, W.J. Pitz, H.J. Curran, A single pulse shock tube study of pentene isomer pyrolysis, Proc. Combust. Inst. 38 (2020), doi:10.1016/j.proci.2020.06.069.
[54] S. Panigrahy, J. Liang, S. Nagaraja, Z. Zuo, G. Kim, T. MacDougall, S.S. Vasu, H.J. Curran, A comprehensive experimental and improved kinetic modeling study on the pyrolysis and oxidation of propyne, Proc. Combust. Inst. 38 (2020), doi:10.1016/j.proci.2020.06.320.
[55] S. Dong, K. Zhang, P.K. Senecal, G. Kukkadapu, S.W. Wagnon, S. Barrett, N. Lokachari, S. Panigrahy, W.J. Pitz, H.J. Curran, A comparative reactivity study of 1-alkene fuels from ethylene to 1-heptene, Proc. Combust. Inst. 38 (2020), doi:10.1016/j.proci.2020.07.053.
[56] S. Nagaraja, G. Kukkadapu, S. Panigrahy, J. Liang, H. Lu, W.J. Pitz, H.J. Curran, A pyrolysis study of allylic hydrocarbon fuels, Int. J. Chem. Kinet. 52 (2020) 964–978.
[57] U. Burke, W.K. Metcalfe, S.M. Burke, K.A. Heufer, P. Dagaut, H.J. Curran, A detailed chemical kinetic modeling, ignition delay time and jet-stirred reactor study of methanol oxidation, Combust. Flame 165 (2016) 125–136.
[58] K. Zhang, C. Banyon, U. Burke, G. Kukkadapu, S.W. Wagnon, M. Mehl, H.J. Curran, C.K. Westbrook, W.J. Pitz, An experimental and kinetic modeling study of the oxidation of hexane isomers: developing consistent reaction rate rules for alkanes, Combust. Flame 206 (2019) 123–137.
[59] K. Fieweger, R. Blumenthal, G. Adomeit, Self-ignition of S.I. engine model fuels: a shock tube investigation at high pressure, Combust. Flame 109 (1997) 599–619.
[60] P. Zhao, C.K. Law, The role of global and detailed kinetics in the first-stage ignition delay in NTC-affected phenomena, Combust. Flame 160 (2013) 2352–2358.
[61] L. Sileghem, V.A. Alekseev, J. Vancoillie, K.M. Van Geem, E.J.K. Nilsson, S. Verhelst, A.A. Konnov, Laminar burning velocity of gasoline and the gasoline surrogate components iso-octane, n-heptane and toluene, Fuel 112 (2013) 355–365.
[62] R. Kumar, A. Singhal, A. Katoch, S. Kumar, Experimental investigations on laminar burning velocities of n-heptane + air mixtures at higher mixture temperatures using externally heated diverging channel method, Energy Fuels 34 (2020) 2405–2416.
[63] H.H. Grotheer, G. Riekert, D. Walter, T. Just, Non-arrhenius behavior of the reaction of hydroxymethyl radicals with molecular oxygen, J. Phys. Chem. 92 (1988) 4028–4030.
[64] J. Vandooren, P.J. Van Tiggelen, Experimental investigation of methanol oxidation in flames: mechanisms and rate constants of elementary steps, Symp. (Int.) Combust. 18 (1981) 473–483.
[65] T. Tsuboi, K. Hashimoto, Shock tube study on homogeneous thermal oxidation of methanol, Combust. Flame 42 (1981) 61–76.
[66] D.L. Baulch, C.T. Bowman, C.J. Cobos, R.A. Cox, T. Just, J.A. Kerr, M.J. Pilling, D. Stocker, J. Troe, W. Tsang, R.W. Walker, J. Warnatz, Evaluated kinetic data for combustion modeling: supplement II, J. Phys. Chem. Ref. Data 34 (2005) 757–1397.
[67] R.S. Timonen, E. Ratajczak, D. Gutman, Kinetics of the reaction between formyl radicals and atomic hydrogen, J. Phys. Chem. 91 (1987) 692–694.
[68] Y. Hidaka, T. Taniguchi, T. Kamesawa, H. Masaoka, K. Inami, H. Kawano, High temperature pyrolysis of formaldehyde in shock waves, Int. J. Chem. Kinet. 25 (1993) 305–322.
[69] P.H. Cribb, J.E. Dove, S. Yamazaki, A kinetic study of the oxidation of methanol using shock tube and computer simulation techniques, Combust. Flame 88 (1992) 186–200.
[70] L.B. Harding, A.F. Wagner, The reaction of atomic hydrogen with the formyl radical, Symp. (Int.) Combust. 21 (1988) 721–728.
[71] J. Li, Z. Zhao, A. Kazakov, F.L. Dryer, An updated comprehensive kinetic model of hydrogen combustion, Int. J. Chem. Kinet. 36 (2004) 566–575.
[72] S.R. Sellevåg, Y. Georgievskii, J.A. Miller, The temperature and pressure dependence of the reactions H + O2 (+M) → HO2 (+M) and H + OH (+M) → H2O (+M), J. Phys. Chem. A 112 (2008) 5085–5095.
[73] A.W. Jasper, S.J. Klippenstein, L.B. Harding, B. Ruscic, Kinetics of the reaction of methyl radical with hydroxyl radical and methanol decomposition, J. Phys. Chem. A 111 (2007) 3932–3950.